Biomass gasification under high solar heat flux: experiments on thermally thick samples

Victor Pozzobon[1] ✉, **Sylvain Salvador**[1], **and Jean Jacques Bézian**[1]

[1]Université de Toulouse, centre RAPSODEE, UMR CNRS 5302, Mines Albi, Campus Jarlard, route de Teillet, 81013 CT Albi Cédex 09, France

In this study, thermally thick samples of beech wood are exposed to radiative heat flux above 1 MW/m^2 (1000 suns). It was motivated by the fact that concentrated solar energy allows to achieve temperatures higher than 1200 °C where char gasification, tar thermal cracking and tar steam reforming can take place. It is achieved using a new experimental device made of an artificial sun and a new reaction chamber, that monitors the sample mass throughout a run and can trap the produced tars using a liquid nitrogen cooled tar condensating device. Thanks to this experimental device, it is possible to compute the average wood consumption rate as well as drying water, char, gas and tar production rates. The produced light gases are also analyzed using microGC. Furthermore, a radiometer is used to monitor surface temperature, which is around 1500 °C. First, a new behavior has been highlighted. Under high radiative heat flux, a char crater which mirrored incident heat flux distribution, is formed inside of the sample. Then, using this device, the impact of two major parameters was tested: wood fiber orientation relative to the solar flux and initial moisture content. Wood fiber orientation (bois de bout and bois de fil) was shown to only have a minor impact on the production rates, gas composition and crater formation. Three initial moisture contents (0, 9 and 55 %wb) were tested. It was shown that increasing the sample moisture leads to direct drying steam gasification of the char produced by the pyrolysis. Moreover, steam also promotes tar steam reforming and therefore decreases the tar yield.

Solar power | Biomass | Gasification | Artificial sun | Experiments
Correspondence: ***victor.pozzobon@mines-albi.fr***

1. Introduction

Mankind is currently facing an increase in energy cost and a climate change problem. Its reliance on fossil fuel has to decrease in favor of renewable energy sources. Among the candidates, biomass pyro-gasification is of note. This process allows to produce carbon neutral gaseous energy vector from biomass. Yet, the transformation of biomass into an energy rich gas is a succession of complex phenomena. It starts with the drying of biomass (1) around 100 °C, where water evaporates from the biomass. Then, pyrolysis takes place around 500 °C. This complex stage turns dry biomass into three main products: light gases (from H_2 to C_3H_8), tars (a mixture of more than 300 molecules (2)) and char (3). Finally, around 800 °C, steam - and to a lesser extend CO_2 - can oxidize char and transform it into syngas (H_2 and CO). This level of temperature also enables tar thermal cracking (4) and tar steam reforming (5). The produced raw gas is therefore potentially a mix of pyrolysis gas, syngas and thermally cracked and steam reformed tars. Once cleaned, filtered or upgraded, this gas can be used in a wide variety of processes: fuel cells, gas turbines, combustion for heat, Fisher Tropsch synthesis. Pyro-gasification is highly endothermic. Classically, heat is supplied by burning a fraction of the inlet biomass feed. Two main drawbacks come with this technique: the efficiency with respect to the biomass is lowered and the produced syngas is diluted by N_2 from the combustion air (6, 7).

Supplying the required heat using solar energy would avoid these drawbacks. Indeed, even on a large scale, solar concentrated power plants can achieve incident heat flux higher than 1000 kW/m^2. Hence, it is possible to reach a temperature of 1200 °C or higher and lead pyrolysis and gasification reactions.

Studies on the combination of biomass gasification and concentrated solar power have been led in the past. However, they mainly focused on reactor scale experiments and modeling. These studies have yielded more insight on the design of the reactors (fixed bed (8–11), fluidized bed (12, 13), cyclonic (14–16)) and the possibilities of the technology. Two reviews of the literature are available on the subject (17, 18). Yet, they do not permit better understanding of biomass and solar power interaction.

The combination of solar energy and biomass still raises several questions at the sample scale. Radiative power has long been seen as a way to achieve high heating rates (1, 19–21). Recently, solar pyrolysis has been studied in order to assess produced char properties (22). The study featured agglomerated wood powder pellets that were suitable to lead a thermally thin experiment, but not to understand the interaction between biomass and solar energy. Furthermore, the behavior a virgin piece of biomass under high solar heat flux has never been studied. Wood is an anisotropic material, thus fiber orientation relative to the incident heat flux may have an impact on the behavior of the sample. The initial moisture content may also alter the sample transformation. Indeed, char produced by biomass pyrolysis can undergo gasification if in contact with steam from drying. Moreover, tar thermal cracking (4) and tar steam reforming (5) may be favored. One could therefore expect a smaller tar yield and a higher direct raw gas production.

A new experimental device was built in order to investigate the effect of the initial moisture content and of the fiber orientation on wood pyro-gasification behavior. The aim of the device is to expose thermally thick beech wood samples to radiative heat flux above 1 MW/m^2 (1000 suns) for a total incident power of 700 W. In order to achieve such high heat flux, an artificial sun was used. Nowadays this kind of device

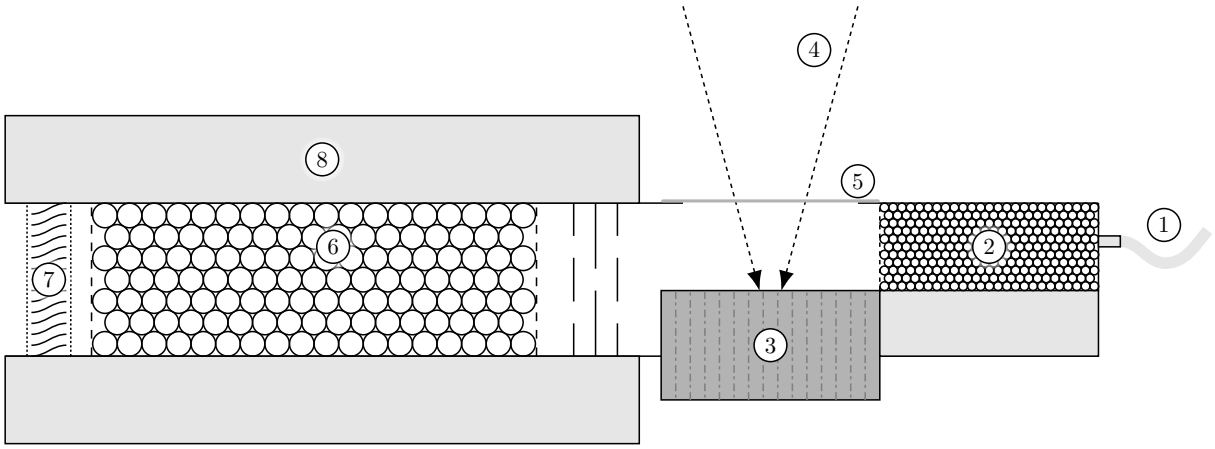

Fig. 1. Schematic of the reaction chamber. 1: nitrogen inlet, 2: porous medium, 3: sample, 4: incident heat flux, 5: quartz window, 6: tar condensing device, 7: cotton trap, 8: insulating material

has become common in the solar application field (23–26). It is basically made of a high power Xenon arc lamp, which produces radiation similar to the solar one. This radiation is focused toward the sample using an elliptical mirror. Two main parameters were varied during this study: initial moisture content, with values of 0 (oven dried), 9 (room equilibrium) and 55 (right after cutting) % wet basis, and fiber orientation, with bois de bout and bois de fil samples.

2. Material and methods

2 1. Experimental apparatus

The aim of the experimental device is to expose a thermally thick biomass sample to high radiative heat flux. Figure 1 provides a schematic of the reaction chamber. The beech wood sample is placed in an enclosure. A quartz window placed above the sample allows the radiative power to enter the enclosure and reach the sample surface. The sample is continuously swept by nitrogen in order to prevent gas and tars released by the sample to reach and soil the quartz window. This nitrogen sweep also ensures that no oxygen is present in the device at any time.

The sweeping nitrogen then carries released gas and tars through a tar condensing system. This system is made of a liquid nitrogen cooled condenser and a cotton trap. The condenser lowers the gas temperature, allowing the tar to condensate into small droplets. These droplets are then captured by the cotton trap. The condensing device is removable. It is also possible to run experiments where tars escape from the reaction chamber. It allows for the quantification of the tar production following a procedure described further.

During a run, the whole system is weighted using a scale. Therefore, the sample mass loss can be accounted for. A pyrometer is set in such a way that it measures sample surface temperature at the focal spot. A set of three thermocouples is placed inside of the sample in order to monitor its core temperature. Finally, part of the gas escaping the condenser and the cotton trap were collected and analyzed using a microGC.

A xenon arc lamp is used as radiative power source. Its radiation is concentrated toward the sample surface using an elliptical mirror. This kind of device has long been used to emulate concentrated solar energy in terms of density and spectrum. It is often referred to as an artificial sun or solar simulator (27). In our case, the biomass sample surface is set at the focal spot of the device. It receives about 700 W of Gaussian distributed radiation with a maximum above 1100 kW/m^2 (Fig. 2) [Pozzobon Salvador - High heat flux mapping - 2015].

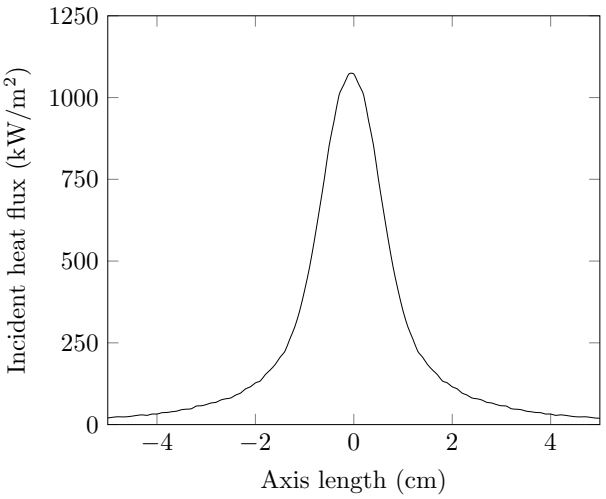

Fig. 2. Incident heat flux on the sample surface

2 2. Samples and varied parameters

The samples used are beech wood cylinders with an height of 5 cm and a diameter of 10 cm. Such massive samples were chosen to behave as slabs during a 5 minutes run. Knowing that wood is an anisotropic material, special care was taken in choosing the wood fiber orientation. Two batches of sample were used for the experiments: a first batch of sample made of bois de bout where the wood fibers are parallel to the cylinder axis (Fig. 3 top), a second made of bois de fil where the wood fibers are perpendicular to the cylinder axis (Fig. 3 bottom).

Sample moisture content is also a parameter that was varied in this work. Three different moisture contents were used for the experiments: 0 %wb, oven dried until mass stabi-

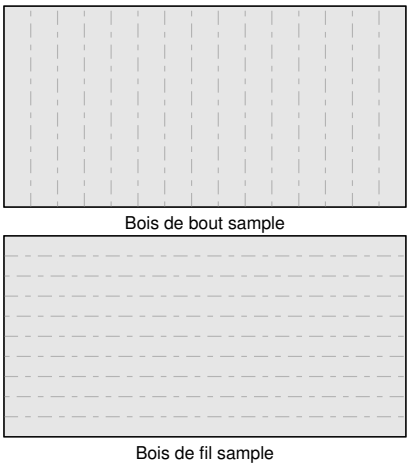

Fig. 3. Samples sketches

lized, 9 %wb, water content stabilized after several month under room condition and 55 %wb, impregnated in water until mass stabilized which is thought to be a representative state of the wood after cutting. Because of the induced swelling and shrinking, the wood density varies with moisture content. The densities are 652 $\pm$ 40, 579 $\pm$ 38 and 535 $\pm$ 8.0 kg of wood/m^3 for, respectively, 0, 9 and 55 %wb initial moisture content samples.

2 3. Experimental procedure

The following steps were strictly followed for every run:

- weighting the sample, the reaction chamber, the condenser and the cotton
- placing of the sample in the reaction chamber
- loading the liquid nitrogen cooled condenser and the cotton trap
- set up of the cell at the focal spot
- exposing the sample for 5 min while collecting gas sample
- cooling the sample under nitrogen sweep for 5 min
- extracting the sample
- weighting the sample, the reaction chamber, the condenser and the cotton

In order to assess for the repeatably, every runs was repeated at least three times.

2 4. Data processing

In order to calculate wood consumption, evaporated water, char, gas and tar average production rates, several mass measurements were taken before and after a run. Before a run, sample mass $m_{sample,\,i}$ and reaction chamber mass $m_{chamber,\,i}$ were measured. After a run, sample mass $m_{sample,\,f}$ and reaction chamber mass $m_{chamber,\,f}$ were measured again. Exposed samples contain a char residue produced by pyrolysis which was not consumed by gasification (Fig. 4). This char was scratched away from the sample and its mass m_{char} was taken. Then, the void left by the char was filled with sand in order to measure the volume of the crater in the wood. The mass of this sand m_{sand} was taken. Knowing, the sand and the wood density, it is possible using Eq. 1 to determine the mass of wood m_{wood} consumed during a run.

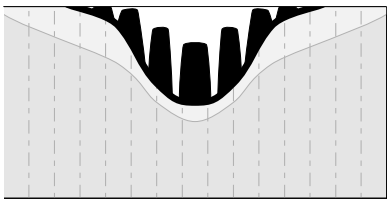

Fig. 4. Schematic cut view of a sample after exposure. Dark gray: moist wood area, light gray: dry wood area, black: char residue

$$m_{wood} = m_{sand}\frac{\rho_{wood}}{\rho_{sand}} \quad \textbf{(1)}$$

Samples were exposed to radiative power in two configurations: with and without tar condensating device. During a run without tar condensating device, gas, tar and water freely escaped from the reaction chamber. Thus, the reaction chamber mass variation $\Delta m_{chamber,\,no\ cond.}$ accounts for the mass of gas produced by the sample m_{gas}, the mass of evaporated water from the sample m_{water} and the mass of tar produced by the sample m_{tar} (Eq. 2).

$$\begin{aligned}\Delta m_{chamber,\,(no\ cond.)} &= m_{chamber,\,f\ (no\ cond.)} \\ - m_{chamber,\,i\ (no\ cond.)} &= m_{gas} + m_{water} + m_{tar}\end{aligned} \quad \textbf{(2)}$$

During a run with the tar condensing device, gas alone escapes from the reaction chamber. Thus, the reaction chamber mass variation $\Delta m_{chamber,\,cond.}$ only accounts for the mass of gas produced by the sample m_{gas} (Eq. 3).

$$\begin{aligned}\Delta m_{chamber,\,cond.} &= m_{chamber,\,f\ (cond.)} \\ - m_{chamber,\,i\ (cond.)} &= m_{gas}\end{aligned} \quad \textbf{(3)}$$

The question of the validity of the comparison between $\Delta m_{chamber,\,no\ cond.}$ and $\Delta m_{chamber,\,cond.}$ may arise. Indeed, these two values are not determined using the same sample. Comparing the reaction chamber mass variation in the two configurations (i.e. $\Delta m_{chamber,\,no\ cond.}$ and $\Delta m_{chamber,\,cond.}$) is possible thanks to the good repeatability of the mass signal (Fig. 5).

From these various measurements, it is possible now to determine the mass of evaporated water released by the sample m_{water}. First of all, m_{wood}, m_{char}, $m_{sample,\,i}$, $m_{sample,\,f}$, m_{gas} and $\Delta m_{chamber,\,no\ cond.}$ are known. We now consider the sample mass variation Δm_{sample}. It accounts for the mass loss of wood m_{wood}, mass loss by drying m_{water} and mass gain by char formation m_{char} (Eq. 4). It possible to access m_{water} using Eq. 4. By knowing m_{water}, it is now possible to access m_{tar} using Eq. 5.

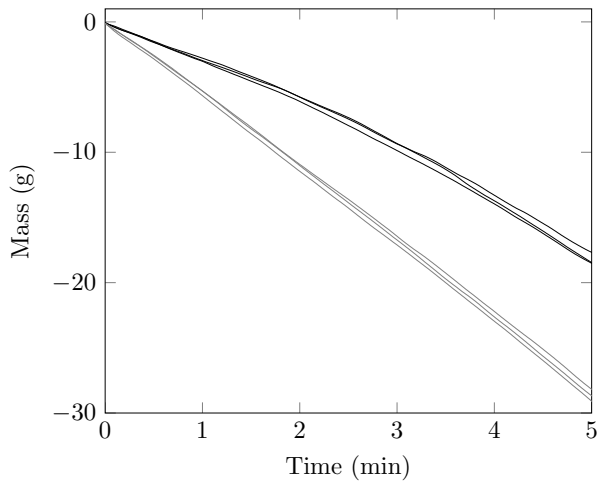

Fig. 5. Three mass signals of reference case sample (9 %wb, bois de bout). Black: with tar condensating device (stopping tar and water), gray: without tar condensating device

$$\Delta m_{sample} = m_{sample,\,f} - m_{sample,\,i} = m_{char} - m_{wood} - m_{water} \quad \textbf{(4)}$$

$$m_{tar} = m_{chamber,\,f\ (no\ cond.)} - m_{chamber,\,i\ (no\ cond.)} - m_{gas} - m_{water} \quad \textbf{(5)}$$

It is therefore possible to calculate the wood consumption and also drying water release, char gas and tar average production rates by dividing the masses by the total run time of 5 min.

Furthermore, by weighting the reaction chamber during a run with the tar condensing, it is possible to determine the evolution of gas production rate.

Three gas samples were also taken at the outlet of the cotton trap at t=0 to 1 min, 2 to 3 min and 4 to 5 min. Gas was then analyzed using a microGC. Average gas composition was also used to calculate the average gas production rate. Indeed, knowing the nitrogen flow rate from the mass flow meter and the stream composition, it is possible to compute the average gas flow rate.

Finally, temperatures were also recorded. Type K and S thermocouples were used to follow temperatures at several points inside of the samples. The repeatability on these measurements was very poor and are not reported here. Nevertheless, it was possible to monitor surface temperature using a bichromatic radiometer within a measurement range from 600 to 1800 °C.

3. Results

3 1. Reference case processing

The case processing is here extensively described for the reference case: bois de bout 9 %wb.

Figure 6 shows the sample after a 5 minutes exposure to radiation. A complex geometry has developed. On the top

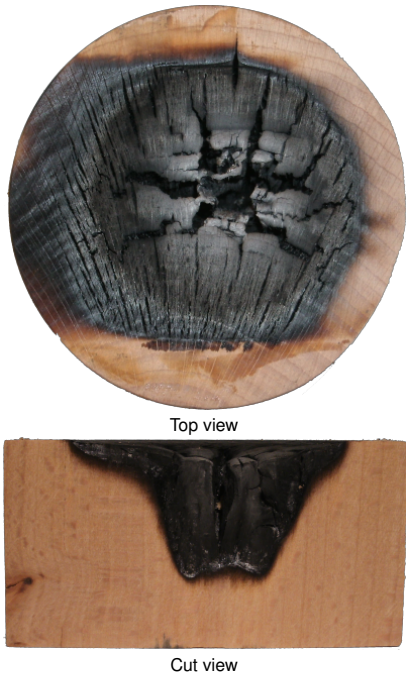

Fig. 6. 9 %wb moisture content bois de bout sample after a 5 minutes exposure

view, one can see a fractured design showing alternatively empty canyons and char rods. The cut view highlights the presence of a charred area with a crater shape. This shape corresponds to the incident heat flux distribution. This crater is filled with standing char rods as illustrated in figure 4.

On average, wood consumption rate is 5.76 g/min (Table 1). It is mainly transformed in to gas (3.65 g/min) and char (1.37 g/min). The production of tar is quite low with only 9 % (0.50 g/min) of the wood being turned into tar. This low tar yield is later explained by tar thermal cracking and steam reforming.

Gas readings show a good repeatability from run to run. Figure 7 reports N_2 free gas composition during a run. One can see that H_2 and CH_4 fractions remain constant throughout a run, while CO fraction decreases from 44 % to 36 % and CO_2 fraction increases from 5 % to 17 %. The explanation for the observed trends in term of gas composition is not straightforward because both tar cracking and tar reforming reactions may participate to the process. Thus, it is beyond the scope of this paper. Other species (C_2H_2, C_3H_8, C_2H_6 and C_2H_4) present in the gas were measured. Their fractions remain stable during a run. The averaged gas production rate was computed from average gas composition. The obtained values are 10 % close to the one obtained using mass measurements. It is thought to be a very satisfactory agreement.

Surface temperature measurements exhibit the same trend (Fig. 8) when repeating the experiment. During the first few seconds of the run, the reading exhibits an overshoot. This overshoot is explained by the high reflectivity of virgin wood around 63 % (28) that blinds the radiometer with reflected light from the Xenon arc lamp. Once the surface is charred, the reflectivity drops to near zero and allows for a proper measurement of the surface temperature. During a run, surface temperature is around 1530 °C, with a slightly

		Time averaged rate (g/min)					Temperature
		Wood	Water	Char	Gas	Tar	(°C)
Bois de bout	0 %wb	7.05 ± 0.48	0.49 ± 0.49	1.74 ± 0.002	4.12 ± 0.07	1.63 ± 0.88	1594 ± 123
	9 %wb	5.76 ± 0.42	1.57 ± 0.43	1.37 ± 0.002	3.65 ± 0.07	0.50 ± 0.82	1530 ± 120
	55 %wb	0.99 ± 0.02	5.89 ± 0.06	0.09 ± 0.002	1.70 ± 0.55	-0.87 ± 0.93	1317 ± 98
Bois de fil	0 %wb	7.09 ± 0.48	0.06 ± 0.49	1.48 ± 0.002	3.64 ± 0.19	1.84 ± 0.98	1616 ± 46
	9 %wb	5.68 ± 0.42	1.09 ± 0.42	1.38 ± 0.002	3.58 ± 0.23	0.49 ± 0.83	1605 ± 90
	55 %wb	1.49 ± 0.03	2.57 ± 0.04	0.17 ± 0.002	1.94 ± 0.20	-0.80 ± 0.98	1426 ± 20

Table 1. Time averaged wood consumption, water, char, gas and tar production rates and average surface temperature for the six configurations

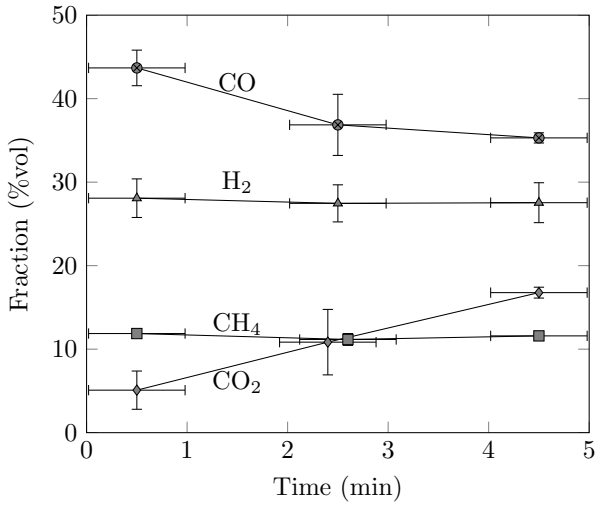

Fig. 7. Gas composition downstream the tar condensating device for the reference case (9 %wb, bois de bout). Triangle: H_2, circle: CO, diamond: CO_2, square: CH_4

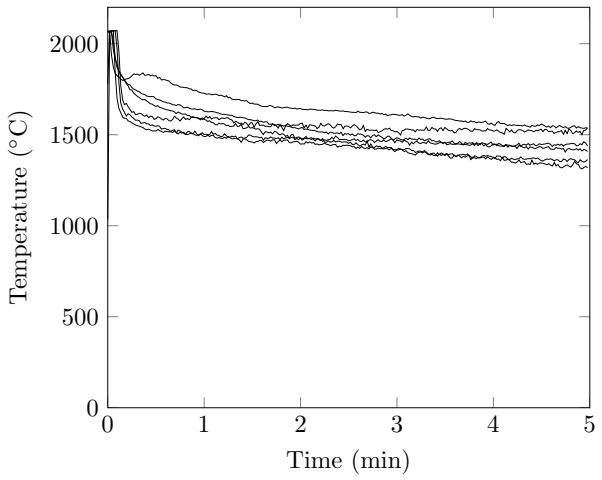

Fig. 8. Surface temperature for 9 %wb initial moisture content bois de bout samples

downward trend. Between runs, ± 120 °C variations are observed. It is known from literature that temperatures higher than 800 °C are required to achieve tar thermal cracking (29) and tar steam reforming (30). Here, the surface temperature is much higher than 800 °C, making tar thermal cracking and tar steam reforming kinetically favored.

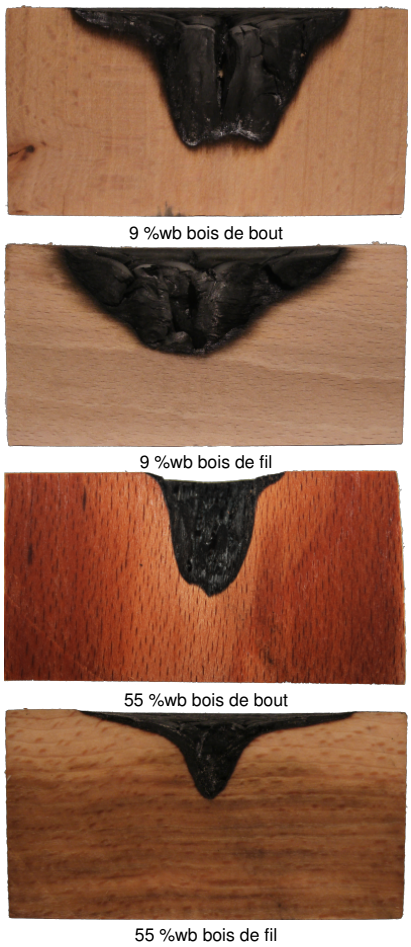

Fig. 9. Samples cut views after 5 minutes exposure

3 2. Crater formation

Cut views of 9 and 55 %wb initial moisture content samples in both fiber directions are reported in figure 9. The 0 %wb initial moisture content samples cut views are not reported because they are very close to those of 9 %wb initial moisture content samples. During a run, sample geometry is significantly modified. Two main behaviors emerge from these

observations. For low initial water content samples, char rods stand inside the crater. For high initial water content samples, a smaller crater is formed, yet no rods stand inside of it. Moreover, cut views show that the transition between wood and char is very sharp. It is therefore possible to consider that the sides of the crater are in fact the location of a pyrolysis front.

- In the case of low initial moisture content, wood shrinking and mechanical failure are thought be at the origin of the char rods formation. Indeed, it is known that during pyrolysis wood shrinks as it turns into char loosing about 70 % of its initial volume (28, 31). In this case, under the high radiative heat flux, the medium undergoes pyrolysis and starts shrinking. As the mechanical constraint grows, some weak spots in the wood structure break. These breaks yield char rods on one hand and canyons on the other. Then the canyons allow the radiation to penetrate even further inside of the sample, providing energy for in depth pyrolysis. In the end, this mechanism yields a crater zone which has a shape close to incident heat flux distribution. Moreover, it is possible using the cut view pictures to determine for the pyrolysis front thickness. The front thickness is about 3 mm for 9 %wb sample and 4 mm for 0 %wb samples.

- In the case of high initial moisture content, steam coming from drying is thought to play a major role in the geometrical evolution of the sample. In the case of low inital moisture content samples, the amount of water released by drying is not high enough to allow for complete char gasification. For high initial moisture content samples, the drying provides enough steam to gasify the char produced by the pyrolysis. Indeed, in order to escape from the sample, the steam has to go through the char which is at temperature far higher than 800 °C. Therefore, char undergoes steam gasification which explains why no char rods are found inside of the crater. Furthermore, the pyrolysis front thickness is small, about 0.5 mm. Indeed, pyrolysis is thought to be shortly preceded by a drying front and is closely followed by a gasification front which immediately consumes the char produced by the pyrolysis front.

There are also similarities in the crater shapes between bois de bout and bois de fil sample (Fig. 9). In the case of 9 %wb initial moisture samples, the char rods inside of the crater are standing upward in both cases. This is surprising given the fact that in the bois de fil cases, the wood fibers are orthogonal to the incident heat flux. One can also note that the average diameter of the char rods is more important in bois de fil samples. Nevertheless, some minor discrepancies remain. Bois de bout samples exhibit a deeper and narrower crater than bois de fil samples. This is due to the fact that wood is an anisotropic material. In the bois de bout cases, the fiber orientation favors heat conduction towards the bottom of the crater inducing sharper shapes. In the bois de fil cases, the fiber orientation favors heat conduction towards the sides of the crater inducing flatter shapes.

3 3. Impact of fiber orientation

Sample fiber orientation varies between two extreme configurations: bois de bout (vertical fibers) and bois de fil (with horizontal fibers). This difference was expected to have an impact on the global behavior of the samples because wood in an anisotropic material. Indeed, the ratio of longitudinal to radial thermal conductivity is about 2 (32). Furthermore, the ratio of the permeability in the same directions is about five thousands (33).

Figure 10 allows for a direct confrontation of the production/consumption rates between the two fiber orientations (data can be found in Table 1). The wood consumption, drying water release, gas, tar and char production rates exhibit close values with only one exception for the 55 %wb cases. In this particular case, water released is much higher for vertical fibers samples than for horizontal ones. It can be explained by the fact that these saturated samples naturally dry in air. Indeed, the channels of the wood come out directly on a pure nitrogen sweeping flow. This setup dramatically promotes drying. In the case of bois de fil samples, the channels of the wood come out on the side of the sample, where there is no sweep. The discrepancy between bois de bout and bois de fil water release rate for 55 %wb samples is explained by a more efficient drying. This was checked in special experiments where sample were expose to the nitrogen sweep without radiative heating.

Figure 11 reports the fractions of the major components of the gas at the outlet of the tar condensating device (data can be found in Table 2). The gas compositions for two fiber orientations are very close for CO, CO_2 and CH_4. The fraction of H_2 may seem to be slightly more important for bois de fil, yet, given the uncertainty, no solid conclusion can be drawn. The same can be stated for gas minor components (Table 3).

Finally, average surface temperatures are very close for bois de bout and bois de fil configurations (Table 1).

3 4. Impact of initial moisture content

The comparison between consumption/production rates with different initial moisture contents is not direct. For instance, the amount of gas produced by a high initial moisture sample is lower than for an initially dry sample. Yet, the amount of converted wood is not the same between these two. In order to solve this problem, the wood consumption rate was chosen as the reference. The water, char, gas and tar production rates were divided by the wood consumption rate, giving yields on dry wood basis (Table 4).

Firstly, as one can see from Table 4, the closure of the mass balance is between 88 and 106 %m which is quite good. Then, as stated before, fiber orientation induces only minor variations in terms of production/consumption rates. Figure 12 reports the relative production yields for bout de fil samples; two main trends emerge from these results:

- An increase in sample initial moisture content leads to a significant reduction of tar production. For 0 %wb

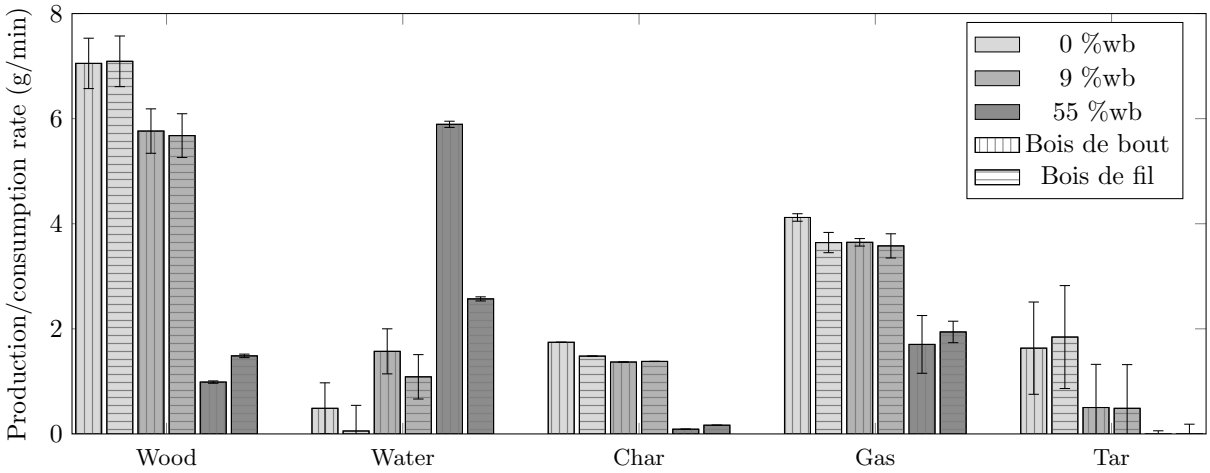

Fig. 10. Production/consumption rates for the six configurations

		Fraction (%vol)			
		H_2	CO	CO_2	CH_4
Bois de bout	0 %wb	25.85 ± 2.06	43.16 ± 2.37	11.09 ± 2.59	13.22 ± 0.53
	9 %wb	27.79 ± 2.31	39.88 ± 2.13	9.45 ± 2.29	11.63 ± 0.44
	55 %wb	37.81 ± 3.42	30.95 ± 3.12	12.15 ± 2.41	8.47 ± 0.95
Bois de fil	0 %wb	30.52 ± 3.32	40.53 ± 1.17	11.23 ± 2.01	11.23 ± 0.49
	9 %wb	31.35 ± 0.89	40.01 ± 3.04	11.78 ± 2.81	10.76 ± 0.75
	55 %wb	36.83 ± 1.69	33.42 ± 2.36	13.51 ± 2.13	8.71 ± 0.53

Table 2. Fractions of major components in the N_2 free gas at the outlet of the tar condensating device averaged throughout a run

		Fraction (%vol)			
		C_2H_2	C_3H_8	C_2H_6	C_2H_4
Bois de bout	0 %wb	1.69 ± 0.48	0.31 ± 0.13	0.34 ± 0.05	2.73 ± 0.29
	9 %wb	1.41 ± 0.28	0.27 ± 0.08	0.26 ± 0.06	2.29 ± 0.31
	55 %wb	1.70 ± 0.38	0.03 ± 0.02	0.11 ± 0.02	1.80 ± 0.32
Bois de fil	0 %wb	1.33 ± 0.19	0.20 ± 0.08	0.32 ± 0.05	2.26 ± 0.39
	9 %wb	1.58 ± 0.51	0.22 ± 0.11	0.29 ± 0.04	2.08 ± 0.20
	55 %wb	1.65 ± 0.26	0.10 ± 0.05	0.20 ± 0.03	1.97 ± 0.12

Table 3. Fractions of minor components in the N_2 free gas at the outlet of the tar condensating device averaged throughout a run

		Water	Char	Gas	Tar	Closure (%)
Bois de bout	0 %wb	0.07 ± 0.07	0.25 ± 0.02	0.58 ± 0.05	0.23 ± 0.14	106
	9 %wb	0.27 ± 0.09	0.24 ± 0.02	0.63 ± 0.06	0.09 ± 0.15	96
	55 %wb	5.97 ± 0.20	0.09 ± 0.01	1.73 ± 0.60	-0.89 ± 0.93	105
Bois de fil	0 %wb	0.01 ± 0.07	0.21 ± 0.01	0.51 ± 0.06	0.26 ± 0.16	98
	9 %wb	0.19 ± 0.09	0.24 ± 0.02	0.63 ± 0.09	0.09 ± 0.15	96
	55 %wb	1.73 ± 0.07	0.11 ± 0.01	1.31 ± 0.17	-0.54 ± 0.65	88

Table 4. Time averaged yields on dry wood basis and mass closure

initial moisture content samples, about 25 % of the wood is transformed into tar. Whereas the tar yield is only 9 % for 9 %wb initial moisture content samples. Tar steam reforming is thought to play a role in this reduction. Indeed, both tar and steam have to escape the medium passing through the crater where temperature are high enough to promote tar steam reforming.

- An increase in sample initial moisture content leads to a major increase in gas production. The gas yield even exceeds 1 for 55 %wb initial moisture content samples. This means that the produced gas mass exceeds the consumed wood mass. It is possible if steam contributes to gas mass through char steam gasification, tars or methane steam reforming.

The reported tar production rates are negative for 55 %wb initial moisture content samples (Table 1). The error associated with these measurements is quite high. Two observations are to be added. It has been qualitatively observed that

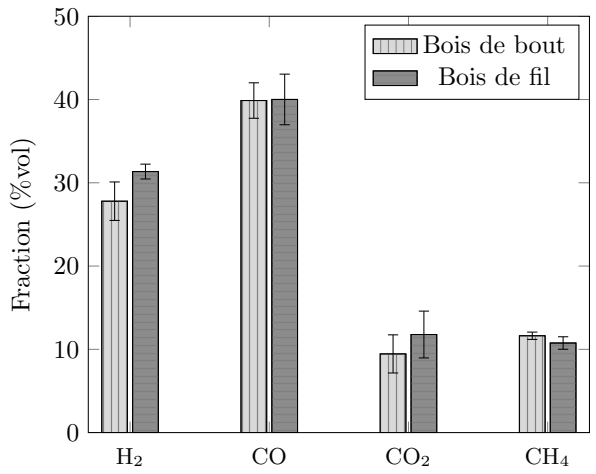

Fig. 11. Major components of the gas for 9 %wb moisture content samples. Dark gray: bois de bout, light gray: bois de fil

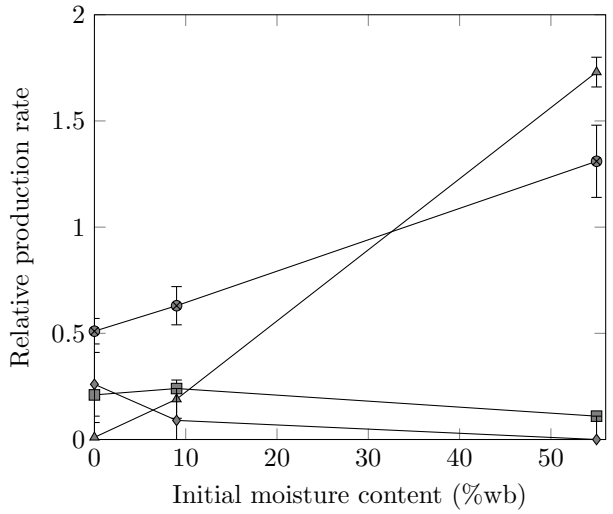

Fig. 12. Relative production rate for bout de fil samples over the range of initial moisture content. Triangle: drying water, square: char, circle: gas, diamond: tar

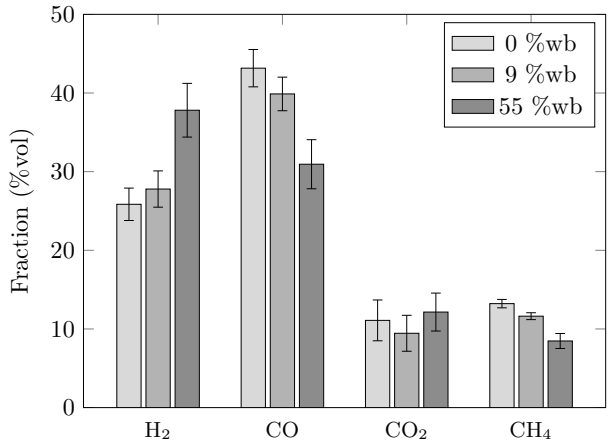

Fig. 13. Major components of the gas for 0, 9 and 55 %wb moisture content bois de bout samples

tar production during these runs is actually very low. Indeed, at the end of these runs the tar condensating device contains only water; no sign of tar can be found in it. Furthermore, the tar cotton trap is superficially colored in light brown, suggesting that only few tars were produced and trapped.

As one can see in figure 13, gas composition varies with sample initial moisture content. Given the error bars, it is possible to consider that 0 and 9 %wb initial moisture content gases have the same composition. Increasing the initial moisture content to 55 %wb leads to an increase in H_2 fraction from 26 to 38 %vol, a decrease in CO and CH_4 fractions from 43 to 31 %vol and from 13 to 8.5 %vol respectively, while CO_2 fractions remains stable. Yet, one should note that the total gas mass production dramatically increases at the same time. The rise in H_2 production is thought to be associated with syngas production by steam gasification of char.

Finally, average surface temperatures drops from about 1600 °C to 1300 °C as biomass initial water content increases from 0 to 55 %wb (Table 1). This is thought to be a consequence of the char steam gasification. Indeed, as char gasification is an endothermic reaction, it can therefore lower the medium temperature.

3 5. Gas production over time

Until now, we only considered time averaged value over a run. The experimental device allows to go one step further and study the gas production rate with time. Gas production rates for the reference case is available in figure 14. Gas production clearly increases with time. It is thought that as the char crater grows as the residence time of tars inside of it increases. Therefore, the contact time between steam and tar before before quenching by nitrogen sweep increases, favoring tar thermal cracking and tar steam reforming leading to gas formation.

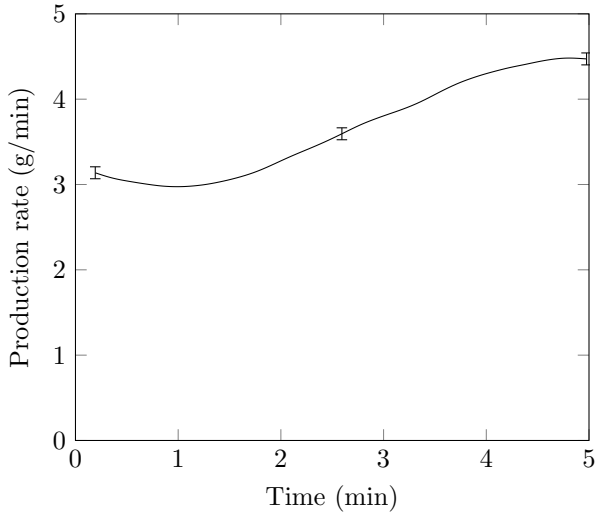

Fig. 14. Gas production rate for the reference case sample (9 %wb, bois de bout)

3 6. Energy balance

Considering that at the process scale, gas, tar and char are the recoverable output energy carriers; it is interesting to evalu-

		Radiative input	Wood HHV input	HHV output in gas	HHV output in tar	HHV output in char	Total HHV output
Bois de bout	0 %wb	700	2233	1176 [40 %]	517 [18 %]	933 [32 %]	90 %
	9 %wb	700	1825	1063 [42 %]	159 [6 %]	732 [29 %]	77 %
	55 %wb	700	312	489 [48 %]	-	49 [5 %]	53%
Bois de fil	0 %wb	700	2246	1023 [35 %]	584 [20 %]	792 [27 %]	82 %
	9 %wb	700	1798	996 [40 %]	154 [6 %]	738 [30 %]	76 %
	55 %wb	700	470	534 [46 %]	-	89 [8 %]	54 %

Table 5. Power distribution (in W) between inputs and chemical outputs. All percentages are on a total power input basis (radiative + wood)

Initial moisture content	Rate (g/min/kW) Wood	Water	Char	Gas	Tar
0 %wb	10.10 ± 0.69	0.39 ± 0.70	2.30 ± 0	5.54 ± 0.19	2.48 ± 1.33
9 %wb	8.17 ± 0.60	1.90 ± 0.61	1.96 ± 0	5.16 ± 0.22	0.71 ± 1.18
55 %wb	1.77 ± 0.04	6.04 ± 0.07	0.18 ± 0	2.60 ± 0.54	-1.19 ± 1.37

Table 6. Averaged wood consumption, water, char, gas and tar production rates per unit of incident power

ate the fraction of the input energy these products can contain. We consider the two energy inputs - incident radiative power and chemical power contained in wood - and the three energy outputs - chemical powers contained in gas, tar and char. It is possible to calculate the power contained in the chemical species flows using their HHV. Wood, tar and char HHVs were taken form the literature with values of 19.0, 19.0 and 32.1 MJ/kg respectively (34)(35)(36). Gas HHV was calculated based on its composition (Tables 2 and 3). Table 5 provides the values of the input power sources and the three outputs powers for the six configurations. One can see that the total power contained in the outputs ranges as high as 90 % for dry samples down to 50 % for high initial moisture content samples. Gas contain about 40 % of the input power in any of the configurations. For high initial moisture content, the retained power is only around half of the input power. It is indeed hindered by drying endothermicity.

Finally, in order to generalize the produced results, the wood consumption, water, char, gas and tar production rates for 1 kW of radiative power were calculated and reported in Table 6 for the different initial moisture contents. This approach should facilitate reactor design for instance. These data were produced by averaging bois de bout and bois de fil contributions because in a reactor samples are generally randomly oriented.

4. Conclusion and perspectives

Thermally thick beech wood samples were exposed to radiative heat flux comparable to the ones found in solar power towers. To do so, a new experimental device was built. It allowed to investigate for behavior of the biomass under heat fluxes higher than 1000 suns.

First, an original behavior has been highlighted. Under high radiative heat flux, sample geometry evolves dramatically during a run. A crater which mirrors incident heat flux distribution is formed. Two mechanisms of crater formation have been proposed: one involving sample shrinking and mechanical failure for low initial water content sample, then other relying on char steam gasification for high initial water content samples.

Then the effect of wood fiber orientation relative to the incident heat flux was questioned. Samples in bois de bout and bois de fil were used to address this question. Surprisingly, the produced results show that varying the sample orientation between these two extrema has only a minor effect on the sample behavior.

The influence of the sample initial moisture content was investigated. It was highlighted that samples containing high initial water content undergo char gasification. They produce 2.6 times more gas than low initial moisture content samples. Furthermore, this gas is richer in H_2 - 36 %vol instead of 26 %. Nevertheless, the input power retained in the products is quite low, around 50 %. The tar yield is close to zero. It has also been shown that samples containing no water produce much more tar than moist samples. For these samples solar pyro-gasification exhibits a very good energy conversion efficiency: the recoverable products contain 90 % and 82 % of the input power (solar + wood).

It can be concluded that the solar pyro-gasification of moist biomass is interesting for enhanced direct H_2 production with reduced tar yield, while solar pyro-gasification of dry biomass is advantageous in the perspective of solar to fuel (gas and tar) conversion.

5. Acknowledgement

This work was funded by the French "Investments for the future" program managed by the National Agency for Research under contract ANR-10-LABX-22-01. We would also like to thank Mickael Ribeiro and Denis Marty for their technical support.

1. Antonio Galgano and Colomba Di Blasi. Modeling the propagation of drying and decomposition fronts in wood. *Combustion and Flame*, 139(1–2):16–27, October 2004. ISSN 0010-2180. .
2. C. Branca, P. Giudicianni, and C. Di Blasi. GC/MS characterization of liquids generated from low-temperature pyrolysis of wood. *Industrial & Engineering Chemistry Research*, 42(14): 3190–3202, July 2003. ISSN 0888-5885. . WOS:000183991400003.
3. Colomba Di Blasi. Combustion and gasification rates of lignocellulosic chars. *Progress in Energy and Combustion Science*, 35(2):121–140, 2009. ISSN 0360-1285. .

4. Thomas A. Milne, Nicolas Abatzoglou, and Robert J. Evans. *Biomass gasifier" tars": Their nature, formation, and conversion*, volume 570. National Renewable Energy Laboratory Golden, CO, 1998.
5. Baofeng Zhao, Xiaodong Zhang, Lei Chen, Rongbo Qu, Guangfan Meng, Xiaolu Yi, and Li Sun. Steam reforming of toluene as model compound of biomass pyrolysis tar for hydrogen. *Biomass and Bioenergy*, 34(1):140–144, January 2010. ISSN 0961-9534. .
6. Paolo De Filippis, Carlo Borgianni, Martino Paolucci, and Fausto Pochetti. Prediction of syngas quality for two-stage gasification of selected waste feedstocks. *Waste Management*, 24(6):633–639, 2004. ISSN 0956-053X. .
7. Nicolas Piatkowski and Aldo Steinfeld. Solar-driven coal gasification in a thermally irradiated packed-bed reactor. *Energy & Fuels*, 22(3):2043–2052, June 2008. ISSN 0887-0624. . WOS:000256057600086.
8. Nicolas Piatkowski, Christian Wieckert, and Aldo Steinfeld. Experimental investigation of a packed-bed solar reactor for the steam-gasification of carbonaceous feedstocks. *Fuel Processing Technology*, 90(3):360–366, March 2009. ISSN 0378-3820. .
9. E.D. Gordillo and A. Belghit. A downdraft high temperature steam-only solar gasifier of biomass char: A modelling study. *Biomass and Bioenergy*, 35(5):2034–2043, 2011. ISSN 0961-9534. .
10. Abdelhamid Belghit. *Etude théorique et expérimentale d'un gazéifieur solaire de matière carbonées en lit poreux mobile*. PhD thesis, Université de Perpignan, 1986.
11. Martin Flechsenhar and Christian Sasse. Solar gasification of biomass using oil shale and coal as candidate materials. *Energy*, 20(8):803–810, 1995. ISSN 0360-5442. .
12. E.D. Gordillo and A. Belghit. A bubbling fluidized bed solar reactor model of biomass char high temperature steam-only gasification. *Fuel Processing Technology*, 92(3):314–321, March 2011. ISSN 0378-3820. .
13. X.T. Li, J.R. Grace, C.J. Lim, A.P. Watkinson, H.P. Chen, and J.R. Kim. Biomass gasification in a circulating fluidized bed. *Biomass and Bioenergy*, 26(2):171–193, 2004. ISSN 0961-9534. .
14. P.v. Zedtwitz and A. Steinfeld. The solar thermal gasification of coal — energy conversion efficiency and CO2 mitigation potential. *Energy*, 28(5):441–456, 2003. ISSN 0360-5442. .
15. Colomba Di Blasi, Carmen Branca, Antonio Santoro, and Raul Alberto Perez Bermudez. Weight loss dynamics of wood chips under fast radiative heating. *Journal of Analytical and Applied Pyrolysis*, 57(1):77–90, January 2001. ISSN 0165-2370. .
16. A. Z'Graggen and A. Steinfeld. Hydrogen production by steam-gasification of carbonaceous materials using concentrated solar energy – V. Reactor modeling, optimization, and scale-up. *International Journal of Hydrogen Energy*, 33(20):5484–5492, October 2008. ISSN 0360-3199. .
17. Nicolas Piatkowski, Christian Wieckert, Alan W. Weimer, and Aldo Steinfeld. Solar-driven gasification of carbonaceous feedstock-a review. *Energy & Environmental Science*, 4(1): 73–82, January 2011. ISSN 1754-5692. . WOS:000285748400006.
18. Ange Nzihou, Gilles Flamant, and Brian Stanmore. Synthetic fuels from biomass using concentrated solar energy – A review. *Energy*, 42(1):121–131, June 2012. ISSN 0360-5442. .
19. Wai-Chun R. Chan, Marcia Kelbon, and Barbara B. Krieger. Modelling and experimental verification of physical and chemical processes during pyrolysis of a large biomass particle. *Fuel*, 64(11):1505–1513, November 1985. ISSN 0016-2361. .
20. Jacques Lédé, Fabrice Blanchard, and Olivier Boutin. Radiant flash pyrolysis of cellulose pellets: products and mechanisms involved in transient and steady state conditions. *Fuel*, 81(10):1269–1279, 2002. ISSN 0016-2361. .
21. Olivier Authier, Monique Ferrer, Guillain Mauviel, Az-Eddine Khalfi, and Jacques Lede. Wood Fast Pyrolysis: Comparison of Lagrangian and Eulerian Modeling Approaches with Experimental Measurements. *Industrial & Engineering Chemistry Research*, 48(10):4796–4809, May 2009. ISSN 0888-5885. . WOS:000266081300016.
22. Kuo Zeng, Doan Pham Minh, Daniel Gauthier, Elsa Weiss-Hortala, Ange Nzihou, and Gilles Flamant. The effect of temperature and heating rate on char properties obtained from solar pyrolysis of beech wood. *Bioresource Technology*, 182:114–119, April 2015. ISSN 1873-2976. .
23. C. Guesdon, I. Alxneit, H. R. Tschudi, D. Wuillemin, and M. Sturzenegger. 1 kW imaging furnace with in situ measurement of surface temperature. *Review of Scientific Instruments*, 77(3):035102, March 2006. ISSN 0034-6748. . WOS:000236739100040.
24. J. Llorente, J. Ballestrin, and A. J. Vazquez. A new solar concentrating system: Description, characterization and applications. *Solar Energy*, 85(5):1000–1006, May 2011. ISSN 0038-092X. . WOS:000290644000029.
25. Joerg Petrasch, Patrick Coray, Anton Meier, Max Brack, Peter Haeberling, Daniel Wuillemin, and Aldo Steinfeld. A novel 50 kW 11,000 suns high-flux solar simulator based on an array of xenon arc lamps. *Journal of Solar Energy Engineering-Transactions of the Asme*, 129(4): 405–411, November 2007. ISSN 0199-6231. . WOS:000250637900008.
26. Daniel S. Codd, Andrew Carlson, Jennifer Rees, and Alexander H. Slocum. A low cost high flux solar simulator. *Solar Energy*, 84(12):2202–2212, December 2010. ISSN 0038-092X. .
27. Jawad Sarwar, Grigoris Georgakis, Robert LaChance, and Nesrin Ozalp. Description and characterization of an adjustable flux solar simulator for solar thermal, thermochemical and photovoltaic applications. *Solar Energy*, 100:179–194, February 2014. ISSN 0038-092X. . WOS:000331007700018.
28. Victor Pozzobon, Sylvain Salvador, Jean Jacques Bézian, Mouna El-Hafi, Yannick Le Maoult, and Gilles Flamant. Radiative pyrolysis of wet wood under intermediate heat flux: Experiments and modelling. *Fuel Processing Technology*, 128:319–330, December 2014. ISSN 0378-3820. .
29. T. Wongchang, S. Patumsawad, and B. Fungtammasan. An Analysis of Wood Pyrolysis Tar from High Temperature Thermal Cracking Process. *Energy Sources, Part A: Recovery, Utilization, and Environmental Effects*, 35(10):926–935, May 2013. ISSN 1556-7036. .
30. Hirotatsu Watanabe, Yosuke Morinaga, and Ken Okazaki. Steam-Reforming Characteristics of Heavy and Light Tars Derived from Cellulose. *Journal of Thermal Science and Technology*, 7(1):180–189, 2012. ISSN 1880-5566. . WOS:000305075400013.
31. Th. Damartzis, G. Ioannidis, and A. Zabaniotou. Simulating the behavior of a wire mesh reactor for olive kernel fast pyrolysis. *Chemical Engineering Journal*, 136(2–3):320–330, March 2008. ISSN 1385-8947. .
32. Guillaume Gauthier. *Synthèse de biocarburants de deuxième génération : Etude de la pyrolyse à haute température de particules de bois centimétriques*. PhD thesis, INPT EMAC, 2013.
33. Eusebe Agoua and Patrick Perre. Mass Transfer in Wood: Identification of Structural Parameters from Diffusivity and Permeability Measurements. *Journal of Porous Media*, 13(11): 1017–1024, 2010. ISSN 1091-028X. WOS:000285561200008.
34. Ayhan Demirbas. Determination of calorific values of bio-chars and pyro-oils from pyrolysis of beech trunkbarks. *Journal of Analytical and Applied Pyrolysis*, 72(2):215–219, November 2004. ISSN 0165-2370. .
35. P. M. Mortensen, J. D. Grunwaldt, P. A. Jensen, K. G. Knudsen, and A. D. Jensen. A review of catalytic upgrading of bio-oil to engine fuels. *Applied Catalysis A: General*, 407(1–2): 1–19, November 2011. ISSN 0926-860X. .
36. L.P.L.M. Rabou, R.J.C. van Leijenhorst, and J.H.O. Hazewinkel. *High efficiency power production from biomass and waste*. ECN Biomass, Coal and Environmental Research, November 2008.